The Impact of GPS Modernization on Standalone User Performance and Integrity with ARAIM

Sam Pullen and Per Enge
Stanford University

Stuart Shaw, Charles Frey, John Frye, and Michael Souder
Lockheed Martin

ABSTRACT

Advanced RAIM, or ARAIM, extends and improves upon the traditional RAIM algorithm to detect and mitigate independent, multiple, and correlated GPS signal faults. While ARAIM depends on multiple redundant satellites in view and will perform best for multi-constellation users, the modernization of the GPS satellite constellation and Operational Control Segment provides a basis for future improvements in ARAIM availability for GPS-only users due to improved ranging accuracy and lower satellite fault probabilities.

This paper quantifies the effects of GPS modernization to evaluate the capability of ARAIM for military dual-frequency (L1-L2) users. Different mixes of GPS satellite types (Blocks IIA, IIR, IIR-M, IIF, and III) are generated to represent future stages of GPS modernization, and different range-error and failure models are constructed for each satellite type. ARAIM simulation results show the performance improvements for military LPV precision approach users as modernization proceeds. In particular, a future constellation of GPS Block III satellites provides significantly higher availability of LPV accuracy and integrity than today's mix of satellites and late-generation Block II satellites. As modernization proceeds, it is likely that sufficient LPV availability will be obtainable from the GPS constellation alone.

1.0 Introduction

GPS users with demanding requirements on the safety, or integrity, of their navigation information now have several options. These include the use of separate correction messages from augmentation systems such as SBAS and GBAS and autonomous integrity verification using Receiver Autonomous Integrity Monitoring, or RAIM. Both of these approaches have advanced significantly in the last decade. In particular, Advanced RAIM, or ARAIM, extends and improves upon the traditional RAIM algorithm to detect and mitigate independent, multiple, and correlated GPS signal faults, making it possible to support applications such as aviation precision approach without requiring real-time integrity messages [1]. However, RAIM and ARAIM rely on redundant ranging measurements for detectability. As a result, recent studies have suggested that multiple GNSS constellations will be required to provide aviation precision-approach availability close to that obtainable from GPS with augmentation [2].

For applications that require the use of GPS only, such as most US military applications and civil applications with GPS-only receivers the ongoing modernization of GPS makes it likely that future ARAIM performance will be significantly better than it is today. GPS modernization enhances ARAIM performance in at least two ways. Improved ranging accuracy, or lower errors under nominal (no-fault) conditions, makes it easier for ARAIM to distinguish faulty measurements from normal ones. Improved integrity, or lower un-alerted failure probabilities, relaxes the missed-detection probability that ARAIM must provide to meet the overall safety requirements for precision approach (or any other application). The future GPS constellation may also be expanded and re-optimized around 27 or 30 primary orbit slots as opposed to today's "Expandable 24" or "24 + 3" constellation of 27 satellites (see [3,4]), but this additional improvement is not considered in this paper.

This paper utilizes an ARAIM simulation model to examine the impact of GPS modernization on ARAIM capability without including other GNSS constellations. Various stages of modernization are considered including today's GPS constellation (as of May 2013), the constellation as it might be in 5 to 8 years once all of the 12 Block IIF satellites have been launched, and a much later version which is completely populated by GPS Block III-era satellites (see [5]).

The Stanford Matlab Algorithm Availability Simulation Tool (MAAST) is used to evaluate and compare the ARAIM performance of these modernization variations. For each variation, the current nominal constellation of 27 satellites is simulated along with the satellite outage scenario present in May 2013, where the B5 (or B1F) slot was empty due to the decommissioning of SVN 35 (PRN 30) in late March [6]. Two different range error models are applied to the various Block II and III satellite types. The first is based on providing near-real-time updates to range error bounds using an ARAIM "Integrity Support Message," or "ISM," which is a separate transmission that updates the health status and error-model parameters for each GPS satellite. The other error model assumes that users only have access to the User Range Accuracy (URA) parameters broadcast within the GPS navigation message, which include quantization errors and are likely to be more conservative than what can be supported by an ISM that is specific to a particular region of operations.

Section 2.0 of this paper gives a brief introduction to ARAIM and its implementation to support aviation precision approach. Section 3.0 describes the simplified model of GPS constellation modernization over time and the resulting combinations of Block IIA, IIR, IIRM, IIF and Block III satellites simulated in this study. Section 4.0 explains how both the ISM-based and URA-based range error models were derived and shows the resulting errors for each satellite type in both cases. Section 5.0 presents the results of ARAIM performance simulations for five military user locations over a (repeatable) 24-hour period of GPS satellite geometries. Section 6.0 summarizes these results and illustrates the performance improvements due to GPS modernization for both error models. Section 7.0 concludes the paper and identifies potential areas for further research.

2.0 ARAIM Concept and Implementation

Advanced Receiver Autonomous Integrity Monitoring, or ARAIM, was developed to both improve the performance of traditional weighted-least-squares RAIM (see [7]) and to explicitly include fault modes other than failures of individual GNSS satellites. Traditional RAIM uses redundant satellite measurements (i.e., more than the minimum of four needed to solve for position in three dimensions and user receiver clock error) to cross-check for individual measurements that disagree from the rest sufficiently to create the potential for unacceptable errors.

Using the multiple-hypothesis approach to integrity risk estimation developed in [8] and extending the "solution separation" approach to traditional RAIM explained in [9], ARAIM evaluates the user protection levels that would result from any hypothesized subset of faulty measurements [11].

A qualitative discussion helps illustrate how ARAIM works and how it extends the capabilities of traditional RAIM. Consider a user with measurements from N satellites denoted as y_i, $i = 1, 2, \ldots, N$ (where $N > 4$) who solves for a four-state position vector x_j, $j = 1, \ldots, 4$, where x_1, x_2, and x_3 represent position in three dimensions and x_4 represents receiver clock error. Let p represent the fault probability of any individual satellite measurement, let q represent the probability of a correlated fault across multiple measurements, and let r represent the required probability that the protection level computed for a given position state bounds the true (unknown) error in that state (note that these probabilities are often expressed per unit of time corresponding to the duration of an operation or part of one).

For high-integrity applications, p needs to be very small: 10^{-3} or below. Therefore, by far the most probable hypothesis (prior to integrity monitoring) is that all measurements are nominal ("healthy" or "non-failed"). Under this H_0 hypothesis, the protection level for position state x_j is computed by extrapolating the nominal position standard deviation σ_j to a sub-allocation of the required probability r (call this r_0) using a Gaussian distribution. Note that this requires errors extrapolated from σ_j and any non-zero mean error μ_j to exceed those given by the true, unknown error distribution for all probabilities equal to or less than r_0.

The next-most-probable hypotheses are the N separate cases of single-satellite faults (call these H_i). If H_i applies, then satellite i has failed, and the best estimate of the resulting user position state error is given by the difference between the position solution with satellite i included (the actual position solution) and the position solution with satellite i excluded (the best estimate of the "true" position solution). This bias error is added to the nominal error of the solution with satellite i excluded to generate the protection level that applies to the H_i hypothesis. This requires extrapolating the nominal error component out to a sub-allocated probability r_i after taking credit for the prior probability p of any individual single-satellite failure.

This "multiple hypothesis solution separation" (MHSS) approach to constructing protection levels can be extended further – it is not limited to single-satellite faults as is the case in traditional RAIM [11]. For example, there are N-choose-2 combinations of independent faults on two different satellites, each combination having probability p^2 because of the assumption that the faults are statistically independent. If the product (N-choose-2) p^2 is non-negligible relative to the total integrity risk R, protection levels for each of these combinations can be computed in the same way as for single-satellite faults. This could be extended to triple-satellite faults if necessary (i.e., if both N and p are large enough). The

hypothesis of a correlated multi-satellite fault is the exception, as a subset of nominal satellites cannot be defined in this case; thus this scenario must be treated as having an undefined protection level (i.e., unbounded errors) with the probability q assigned to this hypothesis. As long as q is small relative to r (which would be the responsibility of GPS or supplemental ground monitoring), this possibility does not impact the overall protection levels.

ARAIM has additional advantages over traditional RAIM beyond explicitly modeling multiple-fault scenarios. As explained in [11], the ARAIM algorithm sub-allocates integrity risk in real time rather than relying on a fixed, pre-determined allocation. ARAIM can thus allocate more risk to fault hypotheses with smaller biases (based on the real-time solution-separation calculation), resulting in more similarity among protection levels across the various fault hypotheses and thus a lower maximum protection level, which is the one that drives operational performance.

The mathematical details of the ARAIM algorithm are not provided here, as they are fully developed in [1], and additional background is given in [2,11] and their references. What is needed to simulate ARAIM performance are the GNSS constellation geometries and satellite types to be used, the nominal error models and failure probabilities that apply to each type of satellite, and the user locations to be considered. These will be defined in the following sections.

3.0 GPS Constellation Evolution Model

As noted above, the GPS constellation simulated in this study is the current "Expandable 24" constellation of 27 satellites given in [3]. As the name implies, this constellation extends the previous 24-satellite baseline constellation by adding three new orbit slots near the existing B1, D2, and F2 slots, providing additional robustness to satellite outages without requiring major changes in constellation maintenance. At any given time, more than 27 satellites are likely to be present, as new satellites are periodically launched before old ones reach end of life. These additional satellites are in "spare" orbit slots that contribute significantly less to user satellite geometries. Therefore, simulating the current 27 primary 27 orbit slots without the spare satellites in place today is considered a reasonable minimum standard for the future. Simulations of one primary satellite outage are also performed, as these will occur on occasion.

Table 1 shows the 26 GPS satellites operating in primary orbit slots as of 16 May 2013. This constellation is called "Baseline-26" in the simulations that follow. The color codes show the relative numbers of Block IIA (4), IIR (12), IIRM (7), and IIF (3) satellites in today's constellation. The most recent Block IIF satellite, SVN 66 / PRN 27, is not shown, as it was enabled for use in mid-June and is now in slot C2 in place of Block IIA SVN 33 / PRN 03, which was moved to spare slot C5 [10]. Note that slot B5, the "expanded" slot near B1, is shown as empty due to the decommissioning of the satellite in that slot (Block IIA satellite SVN 35 / PRN 30) in March [6]. This slot will eventually be filled by a newly-launched satellite. The "Baseline-27" constellation used in the simulations that follow assumes that slot B5 is still filled by a healthy SVN 35 / PRN 30.

Table 2 shows what is called the "Block II Maximum 27" constellation in the following simulations. It projects the continued replacement of older Block IIA and IIR satellites by new Block IIF satellites until all 12 currently-procured Block IIF satellites are fielded in the GPS constellation. Depending on how long it takes for 8 older satellites to reach end of life and how quickly new Block IIF satellites can be launched, a configuration similar to this might occur sometime between 2017 and 2025.

To generate the configuration in Table 2, the oldest 7 satellites in the current primary orbit slots shown in Table 1 (plus the already-failed SVN 35 / PRN 30) are presumed to have ended their lives and been replaced by new Block IIF satellites in the same orbit planes. Like the new SVN 66 / PRN 27, these new satellites would normally be launched into spare slots and later transferred into primary slots in place of the older satellites. In addition, new satellites launched into the three planes with expanded slots are assumed to occupy primary slots 1 – 4 in place of the oldest surviving satellite in those slots, which is moved into the "expanded" slot 5. For example, in the B plane, a new Block IIF satellite was added to replace SVN 35 / PRN 30 but was placed in slot B3, while the satellite currently in slot B3 (Block IIR SVN 44 / PRN 28) was moved to the empty slot B5 because it is the oldest of the four operating satellites currently in slots B1 – B4. A similar change (affecting Block IIR SVN 41 / PRN 14) was made in the F plane.

Two other future configurations are represented in the simulations that follow. One represents the current plan to eventually replace all Block II satellites with Block III satellites. This is called "Block III All 27" and has Block III GPS satellites (likely of several different sub-classes) occupying all 27 primary orbit slots shown in Tables 1 and 2. This would presumably not occur until all 27 Block II satellites shown in Table 2 reach end of life and is thus at least 10 – 15 years in the future. The other alternative considers the possibility that additional Block IIF satellites would be procured to replace the 15 older satellites in Table 2, resulting in a constellation of 27 Block IIF satellites (called "Block IIF All 27"). This could occur somewhat earlier, but it is still well in the future. It is included primarily for comparison with the

Slot	SV (SVN/PRN)	Slot	SV (SVN/PRN)	Slot	SV (SVN/PRN)
A1	IIF-3 (65/24)	C1	IIRM-18 (57/29)	E1	IIR-4 (51/20)
A2	IIRM-15 (52/31)	C2	IIA-25 (33/03)	E2	IIR-10 (47/22)
A3	IIA-28 (38/08)	C3	IIR-11 (59/19)	E3	IIRM-21 (50/05)
A4	IIRM-19 (48/07)	C4	IIRM-14 (53/17)	E4	IIR-7 (54/18)
B1 (e)	IIR-8 (56/16)	D1	IIR-13 (61/02)	F1	IIR-6 (41/14)
B2	IIF-1 (62/25)	D2 (e)	IIF-2 (63/01)	F2 (e)	IIRM-17 (55/15)
B3	IIR-5 (44/28)	D3	IIR-9 (45/21)	F3	IIR-2 (43/13)
B4	IIRM-16 (58/12)	D4	IIA-23 (34/04)	F4	IIR-12 (60/23)
B5 (e)		D5 (e)	IIR-3 (46/11)	F5 (e)	IIA-14 (26/26)

Table 1: 26-Satellite GPS Constellation Configuration as of 16 May 2013

Slot	SV (SVN/PRN)	Slot	SV (SVN/PRN)	Slot	SV (SVN/PRN)
A1	IIF-3 (65/24)	C1	IIRM-18 (57/29)	E1	IIF-new
A2	IIRM-15 (52/31)	C2	IIF-4 (66/27)	E2	IIR-10 (47/22)
A3	IIF-new	C3	IIF-new	E3	IIRM-21 (50/05)
A4	IIRM-19 (48/07)	C4	IIRM-14 (53/17)	E4	IIR-7 (54/18)
B1 (e)	IIR-8 (56/16)	D1	IIR-13 (61/02)	F1	IIF-new
B2	IIF-1 (62/25)	D2 (e)	IIF-2 (63/01)	F2 (e)	IIRM-17 (55/15)
B3	IIF-new	D3	IIF-new	F3	IIF-new
B4	IIRM-16 (58/12)	D4	IIF-new	F4	IIR-12 (60/23)
B5 (e)	IIR-5 (44/28)	D5 (e)	IIR-9 (45/21)	F5 (e)	IIR-6 (41/14)

Table 2: 27-Satellite "Block II Maximum" GPS Constellation Configuration

"Block III All" case to illustrate the potential benefits of the Block III satellite component of GPS modernization.

4.0 GPS Satellite Performance Models

4.1 Satellite Failure Probabilities

As explained in Section 2.0, the probabilities of independent single-satellite failures (p) and correlated multi-satellite failures (q) are key inputs to the ARAIM algorithm. Previous ARAIM simulations based on the existing GPS Block II-era satellites use baseline values of $p = 10^{-5}$ per satellite per hour and $q = 10^{-8}$ per hour (see [2]), and these values are used here as well. Note that the LPV precision-approach phase of flight down to a 200 or 250-ft decision height has a duration of approximately 150 seconds; thus the probabilities per operation are 4.2×10^{-7} per SV and 4.2×10^{-10}, respectively. This value of q is small enough to be neglected relative to the overall LPV integrity requirement of $r = 10^{-7}$ per approach, but this value of p, which applies to each potential satellite failure of the N (typically 7 – 12) satellites in view, is clearly not negligible and must be included in ARAIM protection-level calculations. Fortunately, dual independent satellite failures need not be considered, as the value of $p^2 = 1.8 \times 10^{-13}$ per satellite pair per approach is far smaller than 10^{-7} even after being

multiplied by 66, which is 12-choose-2, or the number of independent satellite pairs with $N = 12$ satellites in view.

The GPS Block III satellites now under development are the first to be subject to strictly-defined user integrity requirements from their conception, and as a result, they are projected to achieve significantly smaller fault probabilities. The current prediction for Block III per-satellite failure probability is slightly below 10^{-6} per hour; thus $p = 10^{-6}$ per satellite per hour (or 4.2×10^{-8} per satellite per approach) is assumed for GPS III. A smaller value for q of 10^{-9} per hour is also assumed, but this change does not affect the results because the number assumed for Block II (10^{-8} per hour) is small enough to be neglected in ARAIM protection-level calculations for LPV precision approaches.

4.2 User Range Error Model

The user range error model used in ARAIM simulations is defined in [2,11] and contains three components:

a) Signal-in-Space (SIS) error (σ_{URA}, σ_{URE}, b_{URA});

b) User receiver error (σ_{air});

c) Tropospheric delay error (σ_{tropo}).

The sigma components of these three error sources are "RSSed" in two ways as part of protection-level calculations. One component of these calculations (σ_{int}) extrapolates one-sigma error to the required integrity sub-allocation, as described in Section 2.0. This component uses the URA values for SIS error bounding and relies on a Gaussian distribution comprised of the URA sigma and bias values to bound the true error distribution out to the extrapolated probability. The other component (σ_{acc}) extrapolates one-sigma error to a separate (and pre-fixed) sub-allocation to continuity risk. Because this calculation is not safety critical to the same degree, the URE sigma is used instead (with an assumed URE bias of zero), where σ_{URE} represents an estimate of the actual error standard distribution and is not deliberately conservative.

Error components (b) and (c) are considered to be the same for both integrity and continuity extrapolations and are also the same for all cases simulated in this study. Only the SIS error contribution changes, and it does so based on both satellite type and error model basis (ISM or URA), as explained below. The user receiver error (b) represents code noise and multipath errors after dual-frequency (L1–L2) differencing to remove ionospheric delays, while the tropospheric delay error represents the error after applying a weather-based model specified in Appendix A of the WAAS MOPS (DO-229D) [12].

4.3 ISM-Based SIS Range Error Model

The starting point for the estimation of URA and URE error values are the ranges of values considered in [2] for civil ARAIM users of L1 and L5 and the studies done to investigate those values by collecting data from the existing Block II satellites (see [13,14] and Chapter 6 of [2]). One difference for military users is that nominal bias errors due to satellite signal deformation should be smaller on P/Y code than they are on C/A code, but without detailed quantification of this effect, it was decided to retain non-trivial URA biases of at least 0.5 meters while setting all nominal (URE) biases to zero.

Table 3 shows the estimates of URA and URE sigma and bias values for the various GPS satellite types that make up what is called the "ISM-based" error model. This name refers to the fact that these errors are lower than what can be broadcast directly by the satellites; thus they must be either pre-fixed or (more likely) separately broadcast to users via the external Integrity Support Message (ISM) mentioned earlier. In addition, the ISM presumed here is one that applies locally to users in a specific region rather than globally, meaning that the error values need not bound the worst user location that can see a given satellite. It may be easier to use a global ISM, and in that case, the values shown here would likely increase somewhat. The objective of the numbers in Table 3 is to specify a model that is close to the best that could be achieved by the combination of ARAIM, backup ground monitoring, and use of one or more ISMs.

Since this study attempts to compare the ARAIM performance of different stages of GPS modernization and thus different satellite types, the relative reductions in URA and URE for newer satellites are important but are difficult to estimate precisely from the available data. The results in [13,14,15] illustrate two key factors: the significant improvement in the Block IIR-class satellites over the earlier Block IIA satellites and the similarity in performance between the few Block IIF satellites now in use and the Block IIR-class satellites. As a result, the Block IIR, IIR-M, and IIF satellites are assigned the same values of σ_{URA} and σ_{URE}. The slightly different URA bias values for these three satellites are based on differences in nominal satellite signal deformation as observed in [16].

SV Type	URA	URA bias	URE
(1) Block IIA	1.25 m	1.00 m	0.90 m
(2) Block IIR	0.80 m	1.00 m	0.60 m
(3) Block IIRM	0.80 m	0.70 m	0.60 m
(4) Block IIF	0.80 m	0.80 m	0.60 m
(5) Block III	0.50 m	0.40 m	0.38 m

Table 3: SIS Components of ISM-Based Error Model

Future Block III satellites are given significantly lower errors because improved performance is expected of them as part of GPS modernization. Regarding typical errors as expressed by URE, the Block III satellites have been developed to meet much stricter accuracy requirements in order to maximize standalone user accuracy. Substantial margin is included to insure that these requirements are met; thus the actual nominal accuracy (without the added margin) is significantly better than the Block IIR and IIF-class satellites.

URA also has stricter requirements than before and is sensitive to infrequent errors that were not a dominant concern for earlier satellites. As noted above, URA needs to bound rare-event errors when extrapolated out to the probabilities required for GPS users. The current minimum probability for satellites flagged as "healthy" is 10^{-5} per satellite per hour [17], which matches the single-satellite fault probability assumed for Block II-class satellites in Section 4.1. When ARAIM computes protection levels based on broadcast URA values, it assumes that the nominal (H_0) hypothesis based on URA bounds all errors out to the single-satellite fault probability p assumed for that satellite, while errors with lower probabilities are assumed to be due to faults (i.e., H_i hypotheses) and are bounded by the solution-separation calculations described in Section 2.0. Because a lower probability of 10^{-6} per satellite per hour is assumed for Block III satellites in Section 4.1, the URA for Block III satellites must bound to a tighter probability despite being lower than the values assumed for Block II satellites. This is deemed acceptable because of the effort made to understand and mitigate satellite errors at the 10^{-5} – 10^{-6} probability level during the GPS III development process.

To examine the sensitivity of the ARAIM results to the assumption of lower Block III errors, two sub-cases of the "III-All-27" satellite scenario are shown in Section 5.0. The first takes credit for the reduced satellite failure probability but uses the same URAs and UREs for Block III as for Block IIF. The second takes credit for both the reduced fault probability and reduced error parameters. The actual improvement expected from Block III satellites is expected to be between these two extremes but closer to the second sub-case.

4.4 URA-Based SIS Range Error Model

Unlike the ISM-based error model, the "(broadcast) URA-based" error model assumes that users do not have access to an ISM and instead derive their SIS error values from the URA indices broadcast in the GPS satellite navigation data (or from fixed, pre-determined values), as defined in [17]. These indices only indicate ranges of URA values, meaning that users must assume the maximum URA value within the range indicated by a given URA index

SV Type	URA	URA bias	URE
(1) Block IIA	1.57 m	1.00 m	0.90 m
(2) Block IIR	1.05 m	1.00 m	0.60 m
(3) Block IIRM	1.05 m (NED = 1.038 m; ED = 0.136 m)	0.70 m	0.60 m
(4) Block IIF	1.05 m (same as IIRM)	0.80 m	0.60 m
(5) Block III	0.66 m (NED = 0.658 m; ED = 0.086 m)	0.40 m	0.38 m

Table 4: SIS Components of URA-Based Error Model (no quantization; *K*-values = 1.0)

and thus suffer from conservatism due to the quantization could be supported by a local ISM (e.g., as noted before, of these indices. In addition, the URA values generated by the GPS satellites and Operational Control Segment (OCS) are more conservative by design than those that they must cover all users that can view a given satellite). Thus, the URA-based error model is significantly more pessimistic than the ISM-based model.

The first step to generating estimates of URA-based errors is to model the algorithm for computing URA values that is being developed for GPS III and the future GPS Advanced Operational Control Segment, or OCX. The input to this algorithm is a 4 × 4 covariance matrix P of satellite on-orbit errors (in three orbit dimensions expressed in RIC coordinates plus clock error). A simplified approach to deriving a representative covariance matrix is developed in [18] and is used in this analysis. In Appendix B of [18], a covariance matrix for a Block IIR-M satellite, satellite SVN 52 / PRN 31, was estimated from 4 weeks of post-processed NGA state estimates in mid-2008. The resulting covariance matrix represents a mixture of ages of data (time since the most recent OCS navigation data upload) but can be used as a reasonable guideline for Block IIR-M satellites (note that it is possible to "age" this covariance further using models of error degradation over time). This matrix can then be re-scaled to represent other satellite types based upon the ratio of variances between the other type in question and the Block IIR-M type. This re-scaling is done here using the ratio of the URE variances (σ_{URE}^2) from Table 3 to form covariance matrices for each satellite type.

The numbers for σ_{URA} in Table 4 are generated from the resulting 4 × 4 covariance matrices P in RIC coordinates based on an algorithm that was provided by Lockheed Martin for this work. To support the CNAV data message, two separate components of σ_{URA} are calculated: URA_{NED} representing "non-elevation dependent" errors and URA_{ED} representing "elevation dependent" errors [17]. LNAV data messages RSS these

SV Type	URA_{NED} or URA	Quant. URA_{NED} or URA / (Index)	URA_{ED}	Quant. URA_{ED} / (Index)	URE	Quant. URE
(1) Block IIA	1.57 m	2.40 m (0)	N/A	N/A	0.90 m	1.0 m
(2) Block IIR	1.05 m	2.40 m (0)	N/A	N/A	0.60 m	0.67 m
(3) Block IIRM	1.038 m	1.20 m (-2)	0.136 m	0.15 m (-8)	0.60 m	0.62 m
(4) Block IIF	1.038 m	1.20 m (-2)	0.136 m	0.15 m (-8)	0.60 m	0.62 m
(5) Block III	0.658 m	0.85 m (-3)	0.086 m	0.11 m (-9)	0.38 m	0.39 m

Table 5: SIS Components of URA-Based Error Model (quantized; *K*-values = 1.0)

SV Type	URA_{NED} or URA	Quant. URA_{NED} or URA / (Index)	URA_{ED}	Quant. URA_{ED} / (Index)	URE	Quant. URE
(1) Block IIA	2.20 m	2.40 m (0)	N/A	N/A	0.90 m	1.0 m
(2) Block IIR	1.47 m	2.40 m (0)	N/A	N/A	0.60 m	0.67 m
(3) Block IIRM	1.45 m	1.70 m (-1)	0.190 m	0.21 m (-7)	0.60 m	0.64 m
(4) Block IIF	1.45 m	1.70 m (-1)	0.190 m	0.21 m (-7)	0.60 m	0.64 m
(5) Block III	0.92 m	1.20 m (-2)	0.120 m	0.15 m (-8)	0.38 m	0.40 m

Table 6: SIS Components of URA-Based Error Model (quantized; *K*-values = 1.4)

two terms together to create a single *URA* ($\equiv \sigma_{URA}$) value to be broadcast in integer (index) form:

$$URA = K_{URA} \times \sqrt{URA_{ED}{}^2 + URA_{NED}{}^2} \qquad (1)$$

where K_{URA} is a constant multiplier (≥ 1.0) that inflates the computed *URA* value as needed to bound rare-event errors. CNAV data messages instead broadcast separate indices for URA_{NED} and URA_{ED}. CNAV data messages are broadcast on L2C and P/Y from Block IIR-M and later satellites and L5C on Block IIF and later satellites. Note that the equations used to compute URA_{NED} and URA_{ED} also have constant multipliers K_{URA_NED} and K_{URA_ED} for the purpose of inflating the computed values to bound rare-event errors (if needed).

The users in this study are assumed to be capable of using CNAV when it is available. CNAV users compute an adjusted URA_{ED} ($AURA_{ED}$) based on their local satellite elevation angle θ ($0 \leq \theta \leq 90$, in degrees) using [17]:

$$AURA_{ED} = URA_{ED} \sin(\theta + 90 \text{ degrees}) \qquad (2)$$

A composite *URA* value is then constructed from URA_{NED}, and $AURA_{ED}$ using equation (1) with $AURA_{ED}$ substituted for URA_{ED} (note that, since $0 \leq \sin(\theta + 90) \leq 1$, $AURA_{ED} \leq URA_{ED}$). As noted above, older satellites (Block IIA and IIR) that only support the legacy navigation data (LNAV) format also apply equation (1) without this adjustment to derive the broadcast *URA* index.

Table 5 shows the *URA*, URA_{NED}, and URA_{ED} values that are used in ARAIM simulations to represent the URA-based error model for the nominal case where all *K*-values in equations (1) and (2) are uninflated (i.e., $K_{URA} = K_{URA\_NED} = K_{URA\_ED} = 1.0$). The original values come from Table 4 but are increased due to the quantization introduced by the fixed ranges of URA values implied by the URA indices that can actually be transmitted [17]. For example, the Block IIR URA derived from Table 4 is 1.05 m, but the smallest index that LNAV can broadcast is 0, which indicates a range from 0 to 2.4 m. Without additional information, such as from an external ISM, the user must assume the highest value in this range, or 2.4 m, which represents a major penalty. The Block IIR-M satellites have the same overall URA broken into URA_{NED} = 1.038 m and URA_{ED} = 0.136 m for CNAV, but the relevant CNAV indices shown in Table 5 result in broadcast values of 1.20 m and 0.15 m, respectively. The CNAV indices have smaller ranges; thus satellites with CNAV have lower but still significant quantization losses.

Table 6 is the same as Table 5 but represents the possibility that *K*-factor inflation is needed to make the URA values resulting from equations (1) and (2) adequately bound rare-event errors. The assumption here

is that an inflation factor of 1.4 is needed for either *URA* (for LNAV satellites) or for both URA_{NED} and URA_{ED} (for CNAV satellites). As a result, the pre-quantized values of *URA*, URA_{NED}, and URA_{ED} from Table 5 are all multiplied by 1.4 in Table 6, and then quantization is re-applied to derive the broadcast values. It is interesting to note that, while the choice of $K = 1.4$ is arbitrary and was selected to represent the need for moderate, but not severe, inflation to bound rare-event errors, the same post-quantization *URA* values would be obtained for any choice of K between 1.28 and 1.54.

Note that quantization is shown for URE (or σ_{URE}) as well as URA in Tables 5 and 6 even though URE is not included in LNAV or CNAV data messages. If URE is fixed or provided by an external ISM, this is not required, but it is preferable in the URA-based error model to avoid reliance on an ISM will allowing URE to increase with URA when a satellite broadcasts URA indices that are higher than normal. A means of calculating "nominal URA" (*NURA*) error values in meters from the broadcast URA indices *I* is given in [17] as follows:

$$NURA = 2^{(1 + I/2)} \quad (3)$$

For LNAV, this relation applies for $I \leq 6$, whereas for CNAV, it applies for $-16 \leq I \leq 6$ to both the NED and ED components of URA (note that indices greater than 6 represent large errors that are not of interest to ARAIM – ARAIM would exclude the satellite instead). While *NURA* values resulting from equation (3) are too conservative to truly represent "nominal" one-sigma errors, empirical modifications of (3) to closely bound the ideal UREs shown in Tables 5 and 6 (and increasing reasonably for higher indices) resulted in the following empirical relations:

IIA, $K = 1$ & 1.4: $\sigma_{URE} = 2^{(I/2)}$ (4)

IIR, $K = 1$ & 1.4: $\sigma_{URE} = 0.67 \times 2^{(I/2)}$ (5)

IIRM & IIF, $K = 1$: $\sigma_{URE} = 2^{(0.3 + I\_NED/2)}$ (6)

III, $K = 1$: $\sigma_{URE} = 2^{(0.15 + I\_NED/2)}$ (7)

IIRM & IIF, $K = 1.4$: $\sigma_{URE} = 0.9 \times 2^{(I\_NED/2)}$ (8)

III, $K = 1.4$: $\sigma_{URE} = 0.8 \times 2^{(I\_NED/2)}$ (9)

For CNAV data messages, note that the index corresponding to URA_{NED}, or *I_NED*, is used in these relations.

4.5 Weighting Matrix in ARAIM Algorithm

The standard ARAIM algorithm described in detail in [1,2] is applied in the ARAIM simulations that follow with one exception. In the standard algorithm, the measurement weighting matrix W used to derive both position solutions and protection levels is computed from σ_{int}, the error sigma extrapolated for integrity bounding and thus based on URA (see Section 4.2). Here, the weighting matrix is computed from σ_{acc} and is thus based on URE instead. The optimal weighting for accuracy purposes (e.g., minimizing confidence intervals covering 50% to 95% of errors) is based on the sigma that best models typical performance, which is why weighting based on σ_{acc} is preferred in this work.

However, an important principle of ARAIM and multiple-hypothesis integrity in general is that the position solution that optimizes accuracy (i.e., minimizes the expected error) is not necessarily the same as the one that optimizes integrity (i.e., minimizes the protection level for a fixed integrity risk probability) [1,8,20]. In previous work [2,11], the difference between URA and URE was not very large, but when the quantized URAs from Tables 5 and 6 are used, this gap can become large. For a few satellite geometries, it was discovered that slightly lower protection levels resulted from URA-based weighting, which implied position solutions optimized for integrity at the expense of accuracy. This was not intended, and as explained above, weighting based on σ_{acc} was chosen to minimize nominal errors as opposed to protection levels.

5.0 ARAIM Simulation Results

5.1 User Locations and LPV Requirements

Table 7 identifies the five U.S. military air bases spread over three continents chosen as locations for evaluation of ARAIM performance in this study. They are widely spread apart and thus see different GPS satellite geometries, even though the GPS constellation being simulated is the same for all. These locations are color-coded in Table 7 to approximately match the ARAIM vertical protection level (VPL) result plots that follow. VPL is plotted instead of protection levels for other state variables because it is most tightly constrained by the LPV requirements and thus determines the availability, or fraction of time that all LPV requirements are met, of LPV precision approach at a particular location.

Two different LPV approach requirements are shown in these results. LPV-250, which has a minimum decision height of 250 ft, requires that the user VPL be no greater

Airbase	Location	Latitude	Longitude
NAS Oceana	SE Virginia, USA	36.82° N	76.03° W
NAS Lemoore	California, USA	36.33° N	119.95° W
MCAS Iwakuni	SW Japan	34.14° N	132.24° E
NAF Mildenhall	SE England	52.36° N	0.48° E
Kandahar AB	SW Afghanistan	31.51° N	65.85° E

Table 7: User Locations for ARAIM Simulations

than a Vertical Alert Limit (VAL) of 50 meters in order to safely fall within the Obstacle Clearance Surfaces that apply to this approach. LPV-200 has a lower minimum decision height of 200 ft and thus requires that VPL be within a tighter VAL of 35 meters [19]. These two bounds are indicated as VAL_{250} and VAL_{200} in the following plots.

The results that follow show significant variations in ARAIM availability for LPV across the five locations in Table 7. This variation is due to differences in the relatively few geometries that give the worst (largest) VPLs. For each location, error model, and satellite constellation, a total of 720 user satellite geometries (one day of GPS satellite orbit propagation at 2-minute intervals) were evaluated and VPLs computed. Significant differences in fewer than 10 of these geometries make the difference between 99% availability and 100% availability, and these differences are intentionally magnified by the plots of sorted VPL shown in the following subsections.

5.2 VPL Results for ISM-Based Error Model

The result plots in this section (Figures 1 – 6) are for the ISM-based error model defined in Section 4.2 without any quantization. As explained above, given the relatively optimistic nature of the ISM-based error model, these results likely represent the best (or nearly the best) performance that can be obtained from ARAIM for the constellations modeled in Section 3.0 and the user locations in Section 5.1.

Figure 1 shows the ARAIM VPL at both NAS Oceana (in Virginia) and NAS Lemoore (in California) for the Baseline-26 constellation shown in Table 1 over 24 hours of repeatable GPS satellite geometries. It shows the typical variation of VPL over time and highlights the differences between these two locations, which represent the best and worst locations for this scenario of the five that were simulated, as shown in Figure 2. The VPL at Oceana varies considerably, from about 10 to 38 meters. It exceeds the 35-meter VAL for LPV-200 at two different times but never approaches the 50-meter VAL for LPV-250, meaning that availability approaching 100% is achieved for LPV-250 but not LPV-200 approaches. (Note that, when all 720 epochs simulated meet the requirement, availability is assured to at least $1 - 1/720 \cong 0.9986$, which is deemed "near 100%" in this paper.) While Lemoore has similar VPLs most of the time, its VPLs rise dramatically and exceed the 50-meter VAL for LPV-250 on two occasions, indicating that neither version of LPV has 100% availability for this constellation.

Figure 2 shows the results for all five (color-coded) locations in Table 7 for the same Baseline-26 constellation using the "sorted VPL" format that will be

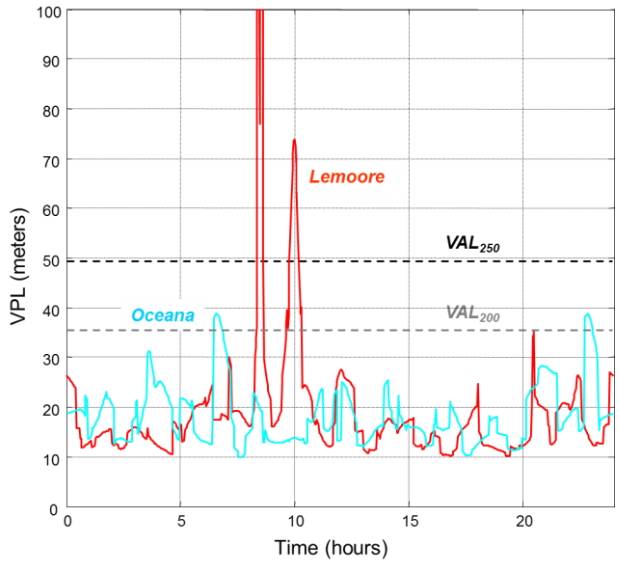

Figure 1: VPL vs. time for NAS Oceana and Lemoore, Baseline-26 Constellation

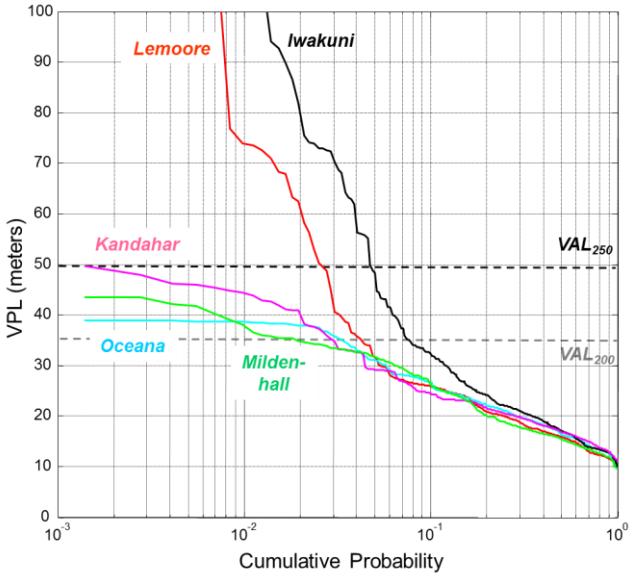

Figure 2: Sorted VPL for Baseline-26 Constellation (ISM-based Error Model)

used in all following plots. This means that the vector of VPL versus time for each location is sorted from smallest to largest and is plotted in that order from right to left. The *x*-axis shows "cumulative probability," meaning the probability that the actual VPL over 720 epochs is larger than the VPL shown on the *y*-axis. For example, in Figure 2, the solid black line representing sorted VPL for MCAS Iwakuni crosses the gray dashed line representing a 35-meter VPL (VAL for LPV-200) at a cumulative probability of roughly 7.5×10^{-2}, or 0.075, telling us that the probability of VPL exceeding 35 meters at Iwakuni is about 0.075 (at least within the simulated results). Conversely, the probability that VPL is below 35 meters is about $1 - 0.075 = 0.925$, giving an approximate

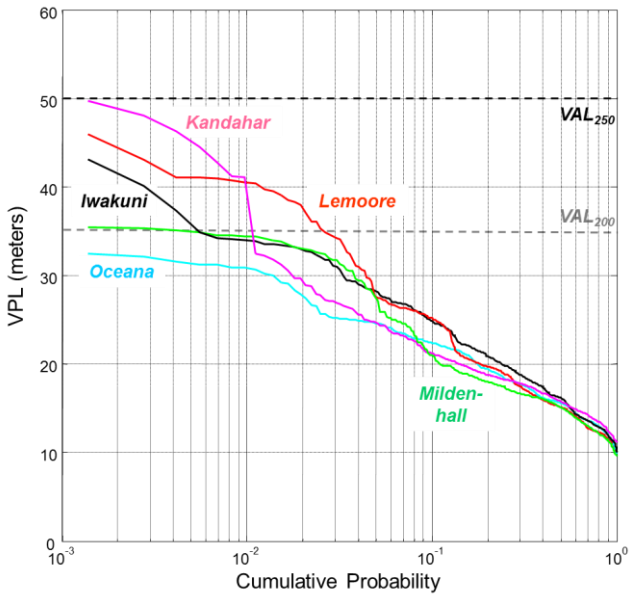

Figure 3: Sorted VPL for Baseline-27 Constellation (ISM-based Error Model)

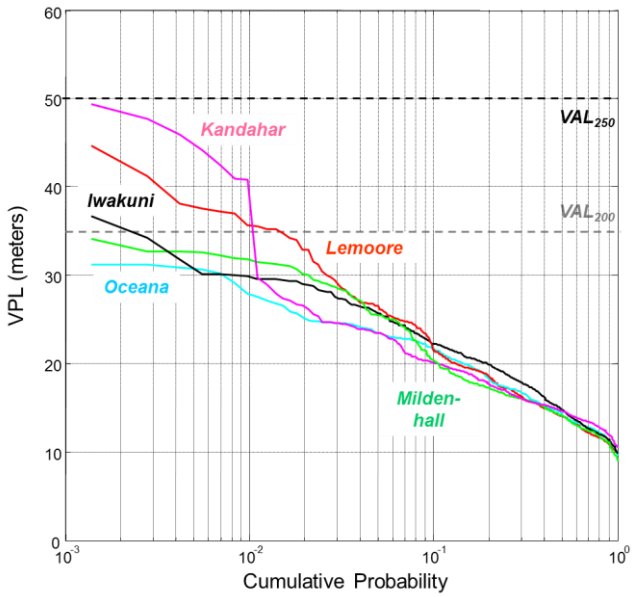

Figure 4: Sorted VPL for II-Max-27 Constellation (ISM-based Error Model)

availability for LPV-200 of 92.5%. Similarly, the VPL curve for Iwakuni crosses the 50-meter VPL line (VAL for LPV-250) at a probability of about 0.045, giving an approximate availability for LPV-250 of 95.5%.

Overall, Figure 2 shows that two locations, Iwakuni and Lemoore, have significantly higher VPLs beyond the 95th percentile than do the other three locations, which all have LPV-250 availabilities approaching 100%. These two locations likely suffer from the absence of the Block IIA satellite in slot B5, which is absent from the Baseline-26 constellation but is included in the Baseline-27 set whose results are shown in Figure 3. The other three locations, Oceana, Mildenhall, and Kandahar, perform much better for the Baseline-26 case, but note that their availabilities for LPV-200 are below 99% (they are about 98%, 97%, and 97%, respectively). This suggests that, even with the optimistic ISM-based error model, availability for today's constellation will not exceed 99% when outages in primary satellite slots are present.

Figure 3 shows the sorted VPL results for the Baseline-27 constellation. Note that the *y*-axis (VPL) scale has changed from a maximum of 100 meters for the Baseline-26 constellation to a maximum of 60 meters for all constellations with 27 satellites. As expected, filling the B5 orbit slot improves performance for all users, some more than others. All five locations have availabilities near 100% for LPV-250, while LPV-200 availability improves to near 100% for Oceana and well above 99% for Mildenhall and Iwakuni. Kandahar and Lemoore improve to a lesser but still significant degree. Kandahar shows a unique "jump" in VPL around the 99th percentile in this plot. This pattern appears for different probabilities in all of the 27-satellite results, which suggests that it is driven by satellite geometry rather than the differing performance of the satellites that make up the constellation.

Figure 4 shows the sorted VPL results for the "Block II Maximum" 27-satellite configuration shown in Table 2. Recall that this scenario replaces the remaining Block IIA satellites and three oldest Block IIR satellites with new Block IIF satellites such that all 12 Block IIF satellites procured to date are in the constellation. Replacing satellites with larger errors in the ISM-based error model (see Table 3) leads to visibly improved performance compared to Figure 3, particularly for Iwakuni, Lemoore, and Mildenhall, but these improvements are not dramatic.

The results for the "Block IIF All" 27-satellite configuration (in which all 27 satellites are Block IIFs) are not shown because the improvement relative to Figure 4 is too small to see easily at the scale of the plots in this paper. In other words, these results are almost identical to those in Figure 4 with very slight improvements in some places. Given the ISM-based error model in Table 3, this is not surprising, because once all satellites are Block IIR or newer, as in Figure 4, the additional improvement from replacing the remaining Block IIR satellites with Block IIF satellites is quite small.

Figures 5 and 6 show the two sub-cases of the "Block III All" 27-satellite configuration (all satellites are future Block IIIs) introduced in Section 4.3. Figure 5 shows the case where only the single-satellite failure probability improvement for Block III (10^{-6} per hour instead of 10^{-5}) is applied, meaning that Block III URA and URE are taken to be the same as for Block IIF. Despite this

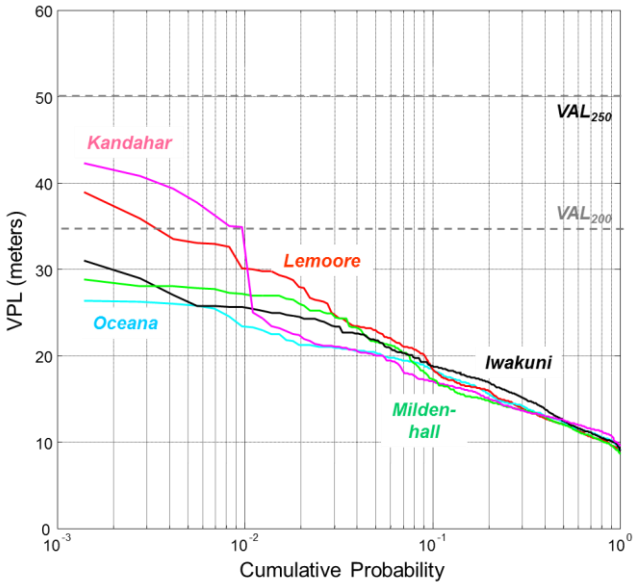

Figure 5: Sorted VPL for III-All-27 Constellation (ISM-based Error Model; $p = 10^{-6}$ improvement only)

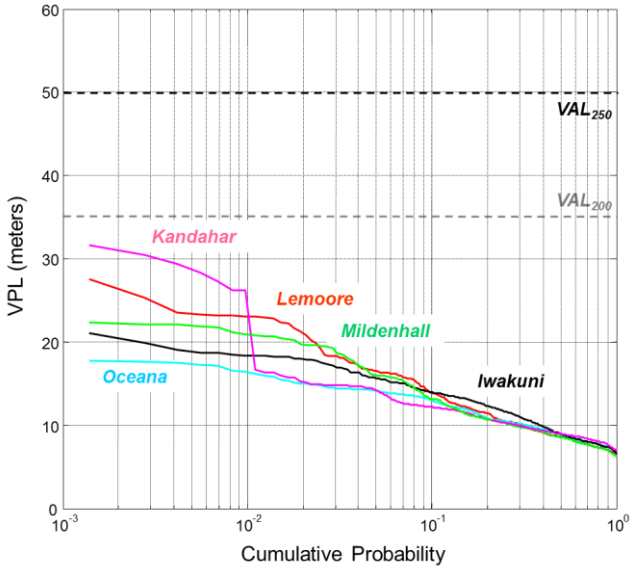

Figure 6: Sorted VPL for III-All-27 Constellation (ISM-based Error Model; *p* and *URA* improvements)

conservatism, the improvement from Figure 4 to Figure 5 is marked, as the left-hand sides of the sorted VPL curves for all five locations (representing the largest VPLs) shift downward by at least several meters. Three of the five locations now have maximum VPLs well below the 35-meter VAL for LPV-200, and Lemoore improves its LPV-200 availability from about 98.5% in Figure 4 to about 99.65%.

Figure 6 represents the case where both the lower fault probability and the lower URA and URE for Block III in Table 3 are included. Now the improvement is dramatic, even compared with Figure 5, as all five locations now have maximum VPLs well below the 35-meter VAL. The better-performing locations (Oceana, Iwakuni, and Mildenhall) have maximum VPLs around 20 meters, suggesting that they would be robust to satellite outages and maintain near-100% availability for LPV-200 in the presence of most single-satellite outages. Note that the improved URA and URE for Block III lower the entire VPL curves from right to left. For example, the median VPL (i.e., VPL at a cumulative probability of 0.5, or the 50th percentile), which is about 17 meters in Figure 2 and 15 meters in Figure 4, drops to only 9 meters in Figure 6.

As noted in Section 4.3, the result in Figure 6 assumes that GPS III can achieve significantly lower URAs than today's Block IIF satellites while simultaneously having these URAs bound errors out to a lower satellite fault probability. This is optimistic but potentially feasible. Even if URA cannot be lowered to the degree suggested in Table 3, any material reduction below the Block IIF values in Table 3 is valuable provided that it is teamed with the lower satellite fault probability to be provided by GPS III.

5.3 VPL Results for URA-Based Error Model (K = 1)

The figures in this section are analogous to those in Section 5.2 but are based on the more-conservative URA-based error model (with all *K* factors set to 1.0) shown in Table 5. Recall that the reliance on satellite data messages to establish URA and URE values adds both conservatism in the estimated error bounds and quantization of these bounds, resulting in significantly higher error bounds (and thus VPLs) from the URA-based error model when compared to the ISM-based model and the results shown in Section 5.2.

Figure 7 is analogous to Figure 2 and shows the URA-based sorted VPL results for the Baseline-26 configuration. For all five users, the results are significantly worse, as expected. The two poorly-performing locations, Iwakuni and Lemoore, are geometry-limited but lose further availability for LPV-250, while the other three locations that previously had near-100% availability for LPV-250 now have availabilities from 97% to 99%.

Figure 8 for the Baseline-27 configuration also shows a major performance loss compared to Figure 3 for the ISM error model. In Figure 8, all five locations have LPV-200 availability well below 99%, while only two locations (Oceana and Mildenhall) have near-100% availability for LPV-250, compared to all five locations achieving this in Figure 3. Figures 7 and 8 suffer greatly compared to the ISM error model results because of the dramatic increase in Block IIA and Block IIR satellite URAs from Table 3 to Table 5. This is mostly due to quantization loss from the minimum URA supported by the LNAV data message

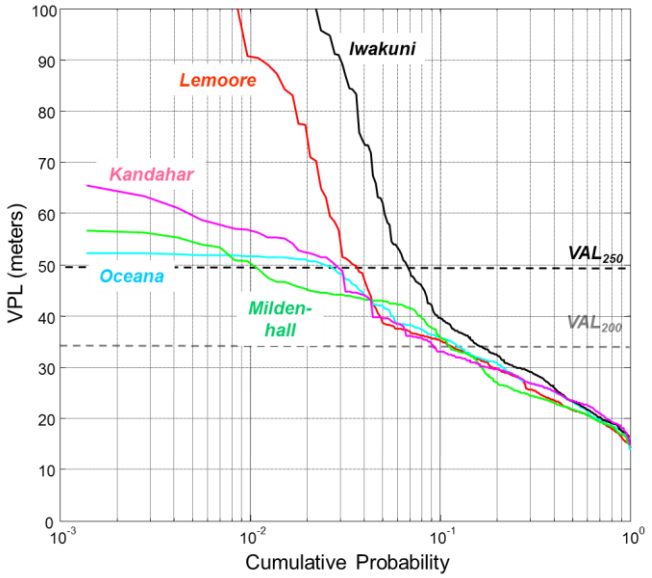

Figure 7: Sorted VPL for Baseline-26 Constellation (URA-based Error Model; *K* = 1)

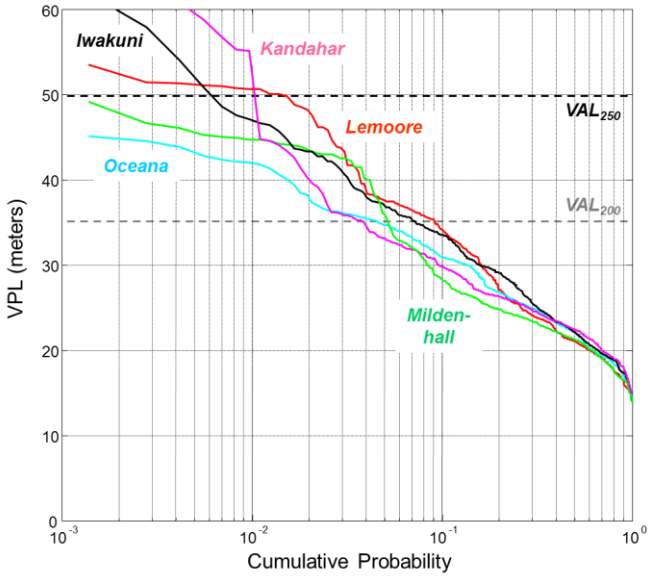

Figure 8: Sorted VPL for Baseline-27 Constellation (URA-based Error Model; *K* = 1)

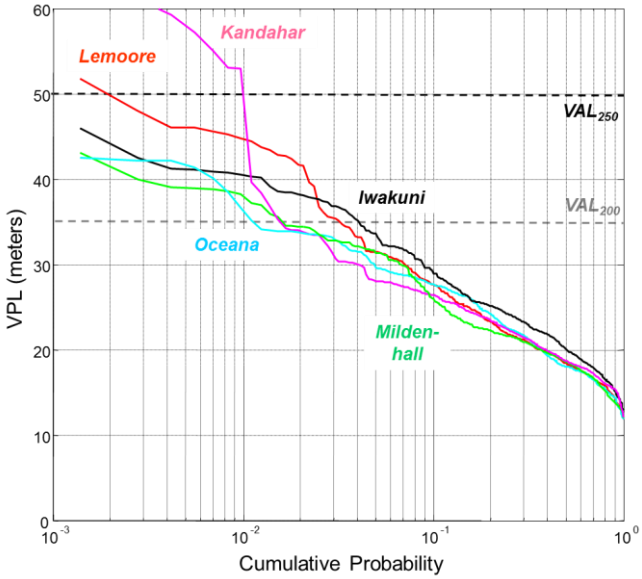

Figure 9: Sorted VPL for II-Max-27 Constellation (URA-based Error Model; *K* = 1)

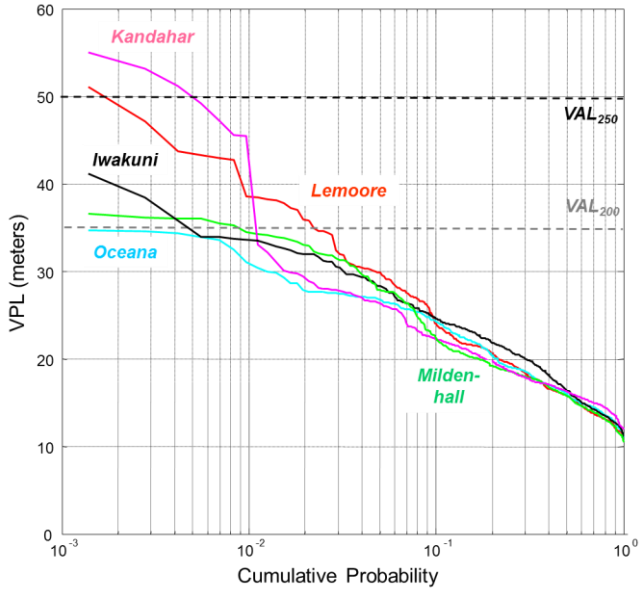

Figure 10: Sorted VPL for IIF-All-27 Constellation (URA-based Error Model; *K* = 1)

(2.4 meters) compared to the pre-quantized URA values for IIA and IIR (1.57 and 1.05 meters, respectively).

Figures 9 and 10 show the URA-based error model results for the "Block II Maximum" and "Block IIF All" 27-satellite configurations, respectively. Figure 9 is analogous to Figure 4 in for the ISM error model and again shows much worse performance because of the many Block IIR satellites remaining in this configuration. Figure 10 does not have an analogous figure for the ISM error model because the "Block IIF All" scenario showed very little improvement over the "Block II Maximum" case. The same is not true for the URA-based error model because the "Block IIF All" scenario replaces the 8 Block IIR satellites in the "Block II Maximum" scenario with Block IIF satellites. This removes all of the satellites severely penalized by LNAV quantization and results in significantly improved performance compared to Figure 9. However, VPL and LPV availability in Figure 10 remain significantly worse than those in Figure 4.

Figures 11 and 12 are analogous to Figures 5 and 6 for the ISM error model and show the results for the "Block III All" 27-satellite constellation; first with only the lower

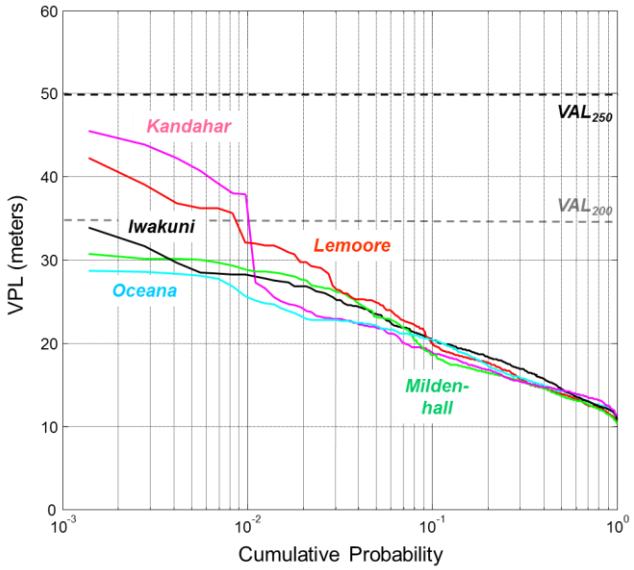

Figure 11: Sorted VPL for III-All-27 Constellation (URA-based Error Model; *K* = 1; *p* improvement only)

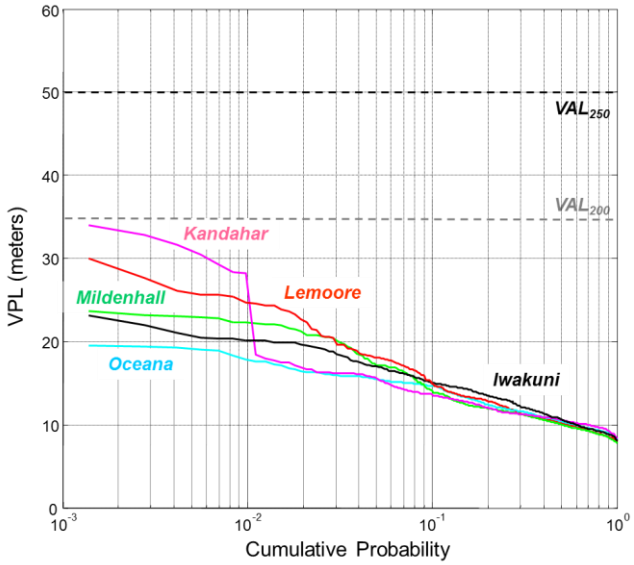

Figure 12: Sorted VPL for III-All-27 Constellation (URA Error Model; K = 1; *p* and *URA* improvements)

satellite fault probability assumed (Figure 11), and then with lower URA and URE also assumed (Figure 12). These results are again worse than the analogous ones for the ISM error model, but this performance loss is less than what is observed in Figures 7 – 10. For example, in Figure 11, VPL at the 90th percentile is about 20 meters, compared to about 18 meters in Figure 5. For this same percentile, VPL in Figure 12 is about 14.5 meters, compared to about 13 meters in Figure 6. In contrast, the 90th-percentile VPL in Figure 9 is about 27 meters, compared to about 21 meters in Figure 4.

What is more important about Figures 11 and 12 is that they improve markedly on Figures 9 and 10 and show that it is possible, if not necessarily desirable, to operate with satellite-broadcast URA values and still achieve high LPV availability with GPS III. In Figure 11, three locations have near-100% availability for LPV-200, and all five achieve this for LPV-250, compared to one and three locations, respectively, in Figure 10. Figure 12, with the improved URA, achieves near-100% availability for all five locations for LPV-200, and three of these locations have substantial margin relative to the 35-meter VAL that provides robustness against satellite outages.

5.4 VPL Results for URA-Based Error Model (K = 1.4)

Figures 13 through 15 in this section are analogous to Figures 10 through 12 in the preceding section. Both sections provide results for the URA-based error model, but this section adds conservatism by applying inflation factors of K = 1.4 to the pre-quantized URA numbers, as explained in Section 4.4 (see Table 6 for the resulting error values). Because the results in Figures 7 through 9 were already quite poor without inflation due to the presence of Block IIA and IIR satellites with high quantization losses, these configurations were simulated but are not re-plotted here.

Figure 13 shows the results for the "Block IIF All" 27-satellite configuration with the inflated URA error model. Comparing these results to those in Figure 10 (without inflation) show a significant degree of additional performance loss, as expected. The 90th-percentile VPL

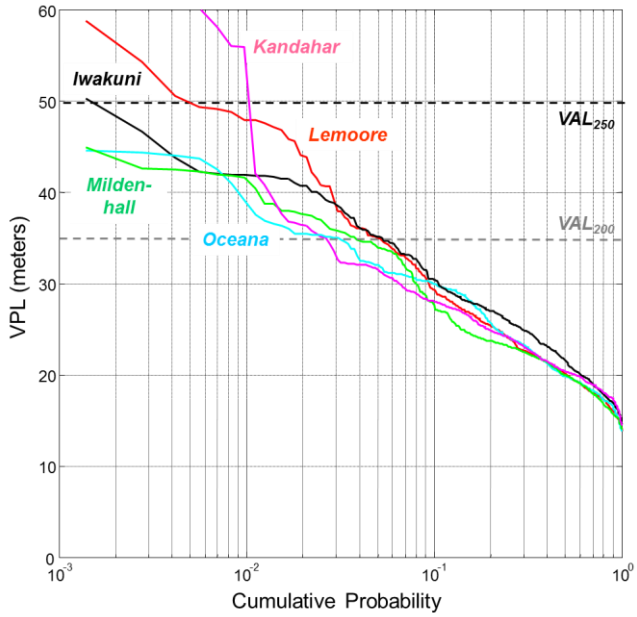

Figure 13: Sorted VPL for IIF-All-27 Constellation (URA-based Error Model; *K* = 1.4)

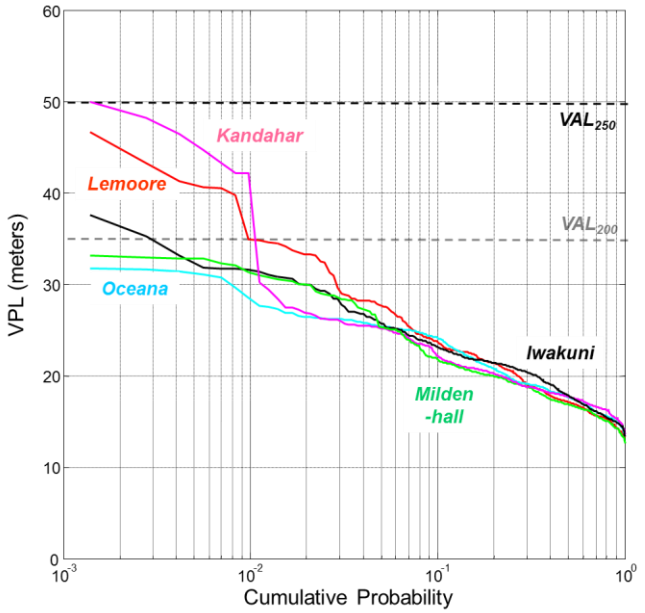

Figure 14: Sorted VPL for III-All-27 Constellation (URA Error Model; *K* = 1.4; *p* improvement only)

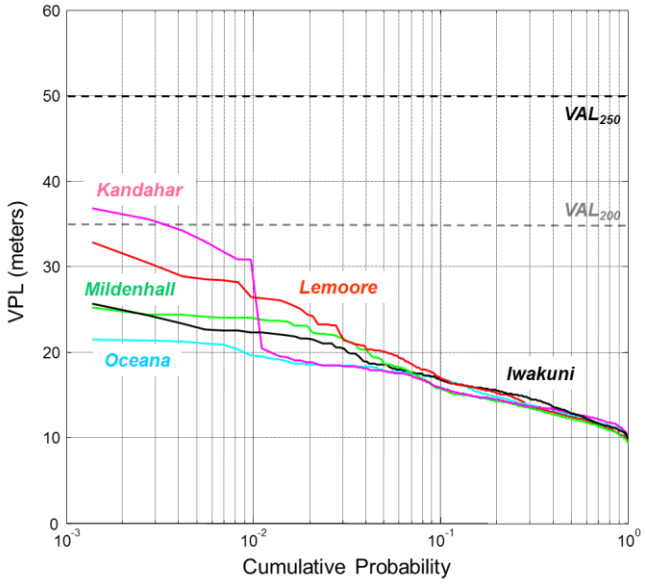

Figure 15: Sorted VPL for III-All-27 Constellation (URA Error Model; *K* = 1.4; *p* and *URA* improvements)

increases from about 23.5 meters in Figure 10 to about 27 meters, while LPV-200 availability is no better than 97.5% in Figure 13 compared to near-100% for one location and above 99% for two others in Figure 10.

Figures 14 and 15 represent the two sub-cases of the "Block III All" 27-satellite configuration and are analogous to Figures 11 and 12. As in previous cases, adopting a constellation of all Block III satellites provides large improvements over all Block II scenarios. In Figure 14, where only the lower satellite fault probability is exploited, the 90th-percentile VPL is reduced to about 23 meters, and all five locations achieve near-100% LPV-250 availability and LPV-200 availability of 99% or better (strictly speaking, Kandahar falls just below 99%). In Figure 15, where the lower URAs are also exploited, the 90th-percentile VPL shrinks to about 16.5 meters, and LPV-200 availability is near 100% for all locations except Kandahar. This performance should be acceptable for most, if not all, military users of ARAIM.

6.0 Results Summary and GPS III Improvements

Table 8 summarizes the results of all ARAIM scenarios simulated in this work, including several for which plots are not shown. The four values listed for each scenario are 90th-percentile VPL, 99th-percentile VPL, LPV-200 availability, and LPV-250 availability. Each value in the table represents the average over the five locations evaluated. In calculating availability, the requirement that the horizontal protection level (HPL) must be less than the horizontal alert limit (HAL) of 40 meters for both LPV-200 and LPV-250 is enforced in addition to the requirements on VPL. While the VPL ≤ VAL constraint dictates availability for almost all satellite geometries, a handful of cases exist in which the VPL constraint is met but the HPL constraint is not. Also note that, in averaging availability across locations and representing it in Table 8, meeting the VPL and HPL requirements over all 720 epochs is treated as "100%" availability rather than the more strictly accurate characterization of "near 100%" availability used in Section 5.0.

An examination of Table 8 reinforces the messages derived from the sorted VPL plots in Section 5.0. The ISM-based error model gives good performance even for today's GPS constellation but may be too optimistic. GPS modernization, in particular the adoption of an all-Block-III satellite configuration, gives near-ideal performance and is much more robust to satellite outages and error bounds that are worse than what is assumed here. The results for the URA-based error model are much worse and essentially require Block III satellite modernization to robustly achieve 99% LPV availability. The URA-based model results highlight the quantization penalty suffered from deriving URA values from satellite-broadcast indices and motivate the use of external ISM broadcasts if possible. Despite this, the performance obtained from Block III satellites make high-availability LPV operations feasible even with conservative error bounds and quantization losses.

While these results were generated for military users of L1 – L2 P/Y code, they are also relevant to civil users of L1 and L5C which have similar (but slightly larger) range errors. Robustness to satellite outages and increased errors is likely to be even more important to civil aviation users of LPV precision approach, as availability of 99.9%

Scenario	90th Pct VPL (m)	99th Pct VPL (m)	LPV-200 Avail.	LPV-250 Avail.
ISM-based Error Model				
Baseline 26	27.0	64.8	95.9 %	98.2 %
Baseline 27	22.9	34.4	99.1 %	99.9 %
Block II Maximum 27	21.1	30.8	99.5 %	99.9 %
Block IIF All 27	20.8	30.3	99.6 %	99.9 %
Block III All 27: Prob. Only	17.8	26.1	99.7 %	99.9 %
Block III All 27: Prob. & URA	13.2	19.0	100 %	100 %
URA-based Error Model; K = 1.0				
Baseline 26	35.8	80.6	87.9%	94.6%
Baseline 27	31.2	45.7	93.9 %	98.8 %
Block II Maximum 27	27.2	39.3	97.7 %	99.6 %
Block IIF All 27	23.4	33.9	99.1 %	99.7%
Block III All 27: Prob. Only	19.6	28.2	99.6 %	99.9 %
Block III All 27: Prob. & URA	14.4	20.6	100 %	100 %
URA-based Error Model; K = 1.4				
Baseline 26	36.7	84.6	86.8 %	94.2 %
Baseline 27	32.0	46.2	93.1 %	98.7 %
Block II Maximum 27	28.9	41.9	96.2 %	99.6 %
Block IIF All 27	26.7	38.6	97.6 %	99.6 %
Block III All 27: Prob. Only	22.8	31.0	99.6 %	99.8 %
Block III All 27: Prob. & URA	16.3	22.4	99.9 %	99.9 %

Table 8: VPL and Availability Results Summary

or better at almost all locations is desirable to support reliable and predictable air traffic operations. Achieving this performance with only the GPS satellite constellation avoids the complexities of reliance on other GNSS constellations that either fall short of GPS performance or are still in the early stages of development.

7.0 Summary and Future Work

This paper examines the potential of ARAIM with GPS modernization to serve aviation users needing high levels of integrity and availability that are not able to make use of navigation satellites other than GPS. ARAIM simulations for both optimistic (ISM-based) and conservative (broadcast-URA-based) error models and several different states of GPS modernization on the way to full Block III equipage have been conducted. These results show the relatively small benefits of replacing today's older Block IIA satellites with Block IIF satellites and the much larger benefits of transitioning from Block II satellites (of any type) to Block III satellites. Results for the Block III scenarios show that LPV availability near 100% (and at least 99% with margin) is achievable for all three Signal-in-Space range error models considered in this paper.

The low VPLs obtained from Block III satellites not only make it possible to achieve high availability for LPV with ARAIM using only GPS satellites. They also provide a high degree of robustness to both satellite outages and increased error bounds that may affect both the ISM and satellite-URA-broadcast implementations of ARAIM. While the VPLs derived from the ISM-based error model may be optimistic, the Block III VPLs for the URA-based error model in Figures 11 and 12 still provide excellent LPV availability, and this remains true after substantial sigma inflation (K = 1.4) is applied in Figures 14 and 15. Quantization loss is a significant factor in the URA-based results; thus implementing an external ISM to transmit less-conservative error values is a key means of

increasing the availability and robustness advantages provided by GPS modernization.

Due to these uncertainties in both future error bounds and GPS constellation orbit evolution, the absolute level of performance that can be expected from ARAIM is difficult to estimate precisely. Future work aimed at reducing these uncertainties would be helpful, but this may take time due to the relatively slow pace of GPS modernization. In the meantime, research into a concept of operations for military aviation using ARAIM and the development of a means by which ISM broadcasts could be integrated into these operations would be valuable. Similar work for the application of ARAIM to civil aviation is already well underway [2,21].

ACKNOWLEDGMENTS

The authors would like to thank Juan Blanch and Todd Walter of the GNSS Laboratory at Stanford University for their expertise and for providing the ARAIM modules of the Stanford MAAST simulation environment. However, the opinions expressed here are solely those of the authors.

REFERENCES

[1] J. Blanch, T. Walter, *et al*, "Advanced RAIM User Algorithm Description: Integrity Support Message Processing, Fault Detection, Exclusion, and Protection Level Calculation," *Proceedings of ION GNSS 2012*, Nashville, TN, Sept. 17-21, 2012, pp. 2828-2849. http://waas.stanford.edu/papers/IONGNSS12_B5_nr7_blanch_rev2.pdf

[2] *Phase II of the GNSS Evolutionary Architecture Study*, Washington, DC, U.S. Federal Aviation Administration, February 2010. http://goo.gl/c323o4

[3] *Global Positioning System Standard Positioning Service Performance Standard*. U.S. Department of Defense, Washington, DC, 4th Edition, Sept. 2008. http://www.gps.gov/technical/ps/2008-SPS-performance-standard.pdf

[4] P. Massatt, F. Fritzen, *et al*, "A Comprehensive Trade Study on GPS Constellation Size and Number of Orbit Planes," *Proceedings of ION GNSS 2006*, Fort Worth, TX, Sept. 26-29, 2006, pp. 2139-2150. https://www.ion.org/publications/abstract.cfm?articleID=6993

[5] W. Marquis, M. Shaw, "Design of the GPS III Space Vehicle," *Proceedings of ION GNSS 2011*, Portland, OR, Sept. 20-23, 2011, pp. 3067-3075. https://www.ion.org/publications/abstract.cfm?articleID=9863

[6] GPS Notice Advisory to NAVSTAR Users (NANU) No. 2013027, May 1, 2013. http://www.navcen.uscg.gov/?Do=gpsShowNanu&num=2013027

[7] T. Walter, P. Enge, "Weighted RAIM for Precision Approach," *Proceedings of ION GPS 1995*, Palm Springs, CA, Sept. 12-15, 1995, pp. 1995-2004. http://waas.stanford.edu/~wwu/papers/gps/PDF/wraim_tfw95.pdf

[8] B. Pervan, S. Pullen, J. Christie, "A Multiple Hypothesis Approach to Satellite Navigation Integrity," *Navigation*, Vol. 45, No. 1, Spring 1998, pp. 61-84. https://www.ion.org/publications/abstract.cfm?articleID=100006

[9] M. Brenner, "Integrated GPS/Inertial Fault Detection Availability," *Navigation*, Vol. 43, No. 2, Summer 1996, pp. 111-130. https://www.ion.org/publications/abstract.cfm?articleID=100053

[10] "The Almanac," *GPS World*, accessed Aug. 7, 2013. http://gpsworld.com/the-almanac/

[11] J. Blanch, A. Ene, *et al*, "An Optimized Multiple Hypothesis RAIM Algorithm for Vertical Guidance," *Proceedings of ION GNSS 2007*, Fort Worth, TX, Sept. 25-28, 2007, pp. 2924-2933. http://waas.stanford.edu/papers/BlanchIONGNSS07.pdf

[12] *Minimum Operational Performance Standards for Global Positioning System/Wide Area Augmentation System Airborne Equipment*, Washington, DC, RTCA DO-229D, Dec. 13, 2006. http://www.rtca.org/store_product.asp?prodid=1101

[13] L. Heng, G. Gao, *et al*, "Statistical Characterization of GPS Signal-In-Space Errors," *Proceedings of ION ITM 2011*, San Diego, CA, Jan. 24-26, 2011, pp. 312-319. http://waas.stanford.edu/papers/LHeng_StatisticalCharofGPSSISErrors_ITM2011_Paper.pdf

[14] C. Cohenour, F. van Graas, "GPS Orbit and Clock Error Distributions," *Navigation*, Vol. 58, No. 1, Spring 2011, pp. 17-28. https://www.ion.org/publications/abstract.cfm?articleID=102540

[15] "Boeing GPS Monthly Navigation Performance Reports," Boeing CDRL A008 for U.S. Air Force, Nov. 2012 - June 2013 (unpublished).

[16] G. Wong, R.E. Phelts, *et al*, "Characterization of Signal Deformations for GPS and WAAS Satellites," *Proceedings of ION GNSS 2010*, Portland, OR, Sept. 21-24, 2010, pp. 3143-3151. http://waas.stanford.edu/papers/WongG_IONGNSS09_SDMCharacterization_paper.pdf

[17] *Navstar GPS Space Segment / Navigation User Interfaces*, El Segundo, CA, U.S. Air Force, Global Positioning Systems Directorate, IS-GPS-200G, Sept. 5, 2012. http://www.gps.gov/technical/icwg/IS-GPS-200G.pdf

[18] R. Braff, B. Bian, C. Shively, "Independent Control Segment URA Monitor for GPS IIIC With Application to LPV 200," *Proceedings of ION GNSS 2010*, Portland, OR, Sept. 21-24, 2010, pp. 3123-3142. https://www.ion.org/publications/abstract.cfm?articleID=9419

[19] *Global Positioning System Wide Area Augmentation System (WAAS) Performance Standard*, Washington, DC, U.S. Department of Transportation / Federal Aviation Administration, GPS-WAAS-PS, 1st Edition, Oct. 31, 2008. http://www.gps.gov/technical/ps/2008-WAAS-performance-standard.pdf

[20] J. Blanch, T. Walter, P. Enge, "RAIM with Optimal Integrity and Continuity Allocations Under Multiple Failures," *IEEE Trans. on Aerospace and Electronic Sys.*, Vol. 46, No. 3, July 2010, pp. 1235-1247. http://ieeexplore.ieee.org/xpl/articleDetails.jsp?arnumber=5545186

[21] J. Blanch, T. Walter, *et al*, "Critical Elements for a Multi-Constellation Advanced RAIM," *Navigation*, Vol. 60, No. 1, Spring 2013, pp. 53-69. http://ion.org/publications/abstract.cfm?jp=j&articleID=2591